3D Printed "Kirigami"-Inspired Deployable Bi-Focal Beam-Scanning Dielectric Reflectarray Antenna for mm-Wave Applications

Yepu Cui, *Student Member, IEEE*, Ryan Bahr, Syed A. Nauroze, Tingyu Cheng, Thamer S. Almoneef, *Member, IEEE*, and Manos M. Tentzeris, *Fellow, IEEE*

***Abstract*— This article presents a state-of-the-art 3-D-printed dielectric reflectarray antenna featuring one-shot deployability and wide-angle beam-scanning ability. The design is enabled by a series of a "kirigami"-inspired two-stage snapping-like element structure that can be retracted by 66% to save space. The prototype is fabricated with a stereolithography (SLA) 3-D printing method with the Formlabs Flexible 80A photopolymer. A bifocal phase distribution method is utilized to optimize the RF performance of the array, realized −30° to −10° and 10° to 30° beam-scanning ability. The outcome of this work demonstrated a high-performance dielectric reflectarray design with ease of fabrication for 5G and satellite communication applications.**

***Index Terms*— 3-D printing, additive manufacturing, antenna arrays, deployable reflectarrays, dielectric reflectarrays, dielectric resonate antennas, flexible electronics, kirigami, origami.**

I. Introduction

HIGH-performance antennas are critically important in modern wireless applications, such as 5G communications, satellite communications, long-range RFID, remote sensing, and so on. Parabolic reflectors and phased arrays are two of the most commonly used topologies for applications requiring narrow beams and high-gain antenna systems. However, parabolic reflectors are bulky, expensive, and hard to fabricate especially above mm-wave frequencies due to their curved profile. Although phased arrays typically require individual tunable phase shifters, power amplifiers, and complex feeding networks that dramatically increase their cost and difficulty of design, they feature significant additional beam steering capabilities. Reflectarray antennas combine some of the best features of both parabolic reflectors and phased array antennas, with the advantage of planar profile, relatively low cost, and ease of fabrication, and can realize wide scan angles without any active components and feeding networks [1]. In addition, planar reflectarray antennas can be transformed to foldable designs utilizing origami-inspired structures [2], membrane [3], or inter-PCB hinges [4], making reflectarray antennas ideal for satellite communication systems. To achieve a dynamic radiation pattern with a reflectarray antenna, mechanical tuning techniques can be utilized by rotating the feed source [5], [6]. In recent years, a bifocal design has proven to be an efficient method to improve the reflectarray scanning range [7], [8], [9].

One of the most significant challenges for mm-wave and terahertz reflectarrays is to reduce conductor losses caused by the metallic phase-shifting elements [10]. In recent years, significant work has been undertaken on dielectric reflectarrays, eliminating conductor losses by replacing the metallic phase shifters with high-dielectric phase delay structures. The phase delay can be tuned by changing the height of each element [11], [12], [13], [14], [15] or changing the effective permittivity of each area [16], [17]. Dielectric reflectarrays have demonstrated several advantages over traditional PCB-based reflectarrays: 1) eliminate conductor losses in the metallic resonant patch elements; 2) much wider bandwidth as dielectric structures are generally not frequency selective; and 3) low cost and ease of fabrication by utilizing 3-D printing and molding processes. However, most of the dielectric reflectarray designs are using a stub-shaped structure as an element, and they are utilizing rigid polymers to fabricate the design, which effectively eliminating the use of current deployable reflectarray techniques, thus preventing them from being able to retract to smaller volume. Subsequently, current dielectric reflectarrays will occupy substantially more space than traditional microstrip-based designs. The lack of deployability and retractability will limit the applicable scenarios for dielectric reflectarrays significantly.

In this article, a novel "kirigami"-inspired dielectric reflectarray is presented featuring high gain, wide bandwidth, beam-scanning ability, and deployability. This article is an extension of previous work [18] with the following new contents: this article has a new bifocal design with a beam-scanning ability of −10° to −30° and 10° to 30° enabled by a phase

Manuscript received 29 December 2021; revised 24 May 2022; accepted 27 July 2022. Date of publication 23 August 2022; date of current version 6 October 2022. This work was supported in part by the Deputyship for Research and Innovation, Ministry of Education, Saudi Arabia, under Project 785; and in part by the Deanship of Scientific Research, Prince Sattam Bin Abdulaziz University, Al-Kharj, Saudi Arabia. *(Corresponding author: Yepu Cui.)*

Yepu Cui, Ryan Bahr, Syed A. Nauroze, Tingyu Cheng, and Manos M. Tentzeris are with the School of Electrical and Computer Engineering, Georgia Institute of Technology, Atlanta, GA 30339 USA (e-mail: ycui80@gatech.edu; rbahr3@gatech.edu; nauroze@gatech.edu; tcheng32@gatech.edu; etentze@ece.gatech.edu).

Thamer S. Almoneef is with the Electrical Engineering Department, College of Engineering, Prince Sattam Bin Abdulaziz University, Al-Kharj 11942, Saudi Arabia (e-mail: t.almoneef@psau.edu.sa).

Color versions of one or more figures in this article are available at https://doi.org/10.1109/TAP.2022.3199501.

Digital Object Identifier 10.1109/TAP.2022.3199501

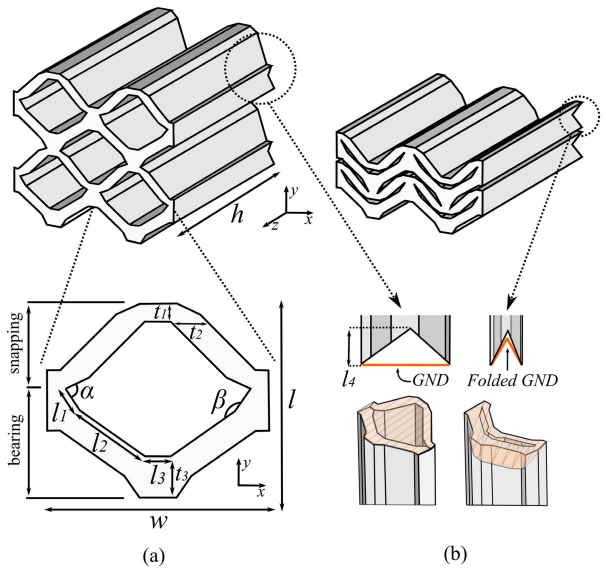

Fig. 1. Element design. (a) Perspective view of the deployed structure and top view of an element. (b) Perspective view of the folded structure and a detailed schematic of the ground plane retraction mechanism.

optimization method. The deployable element structure was characterized and simulated to analyze the mechanical performance as well. The prototype was fabricated with a new stereolithography (SLA) 3-D printable material Formlabs Flexible 80A with much better durability. A thorough characterization for this material was performed from 26 to 40 GHz.

II. Element Design and Analysis

A. Mechanical Design

To realize a deployable dielectric reflectarray with minimum folded volume, we present a novel "snapping-like" structure inspired by monolithic mechanical metamaterials [19], as well as kirigami [20], a variation of origami involving cut sections. To make sure an accurate phase-shifting response and geometry placement for reflectarray design, the element will be built, simulated, and fabricated in a "deployed" configuration.

Fig. 1(a) shows the element design that consists of two segments: a snapping segment and a bearing segment, forming a bistable mechanism. The structure is designed to be actuated with an electric motor or a mechanical switch. The phase response of the reflected wave can be controlled by changing the height h of the element, while each element will have the same cross-sectional dimensions. The dimensions of the element are defined by four lengths l_1, l_2, l_3, and l_4; three dielectric thicknesses t_1, t_2, and t_3, and two angles α and β. As discussed in [18], "another advantage of this design, as compared with a rhomboid-shaped structure, is that it minimizes the total width w variation across retracted and deployed states, resulting in a Poisson ratio close to zero. This means that the reflectarray will not expand or contract along the X-axis during deployment and operation. This is mostly due to angle α and length l_1 that create a triangle-shaped hinge, which allows the snapping segment to "snap" onto the bearing segment. The bottom cutout with depth l_4, as shown in Fig. 1(b), is to facilitate a foldable ground plane

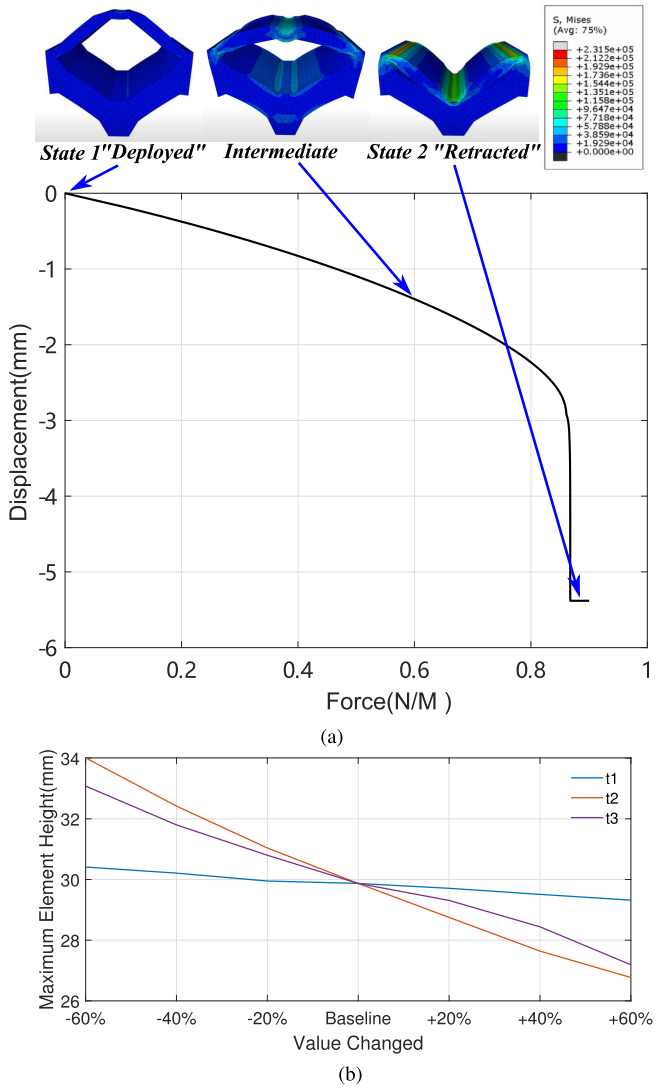

Fig. 2. Mechanical simulation results. (a) Force versus displacement, from "deployed" stage to "retracted" stage. (b) Maximum element height versus geometry parameters t_1, t_2, and t_3 sweep around the design baseline values.

underneath the reflectarray." The dimensions of the element are chosen as: $l_1 = 1$ mm, $l_2 = 2.9$ mm, $l_3 = 1$ mm, $l_4 = 2$ mm, $\alpha = 82°$, $\beta = 160°$, $t_1 = 0.6$ mm, $t_2 = 1.2$ mm, $t_3 = 1.7$ mm, $w = 8.11$ mm, and $l = 7.35$ mm, to display good foldability while maintaining an area less than $1\lambda^2$ to ensure an accurate phase distribution.

The material utilized in this design is Formlabs Flexible 80A, a photopolymer with better printability and durability than the previous [18] Flexible FLGR02. This flexible photopolymer is a "rubber-like" elastomer with Young's modulus of 4.4 MPa. The material is simulated based on 80A durometer rubber with Poisson's ratio of 0.45. The structure is simulated and optimized in Abaqus CAE 2019 with a finite-element method (FEM) solver. The mechanical response of the structure is shown in Fig. 2(a). The displacement is defined as the distance of the snapping segment traveled alone z-axis when pressure applied on top of it. The color on the 3-D structure indicates the Von Mises stress distribution with red color showing the areas with the highest stress. When applying

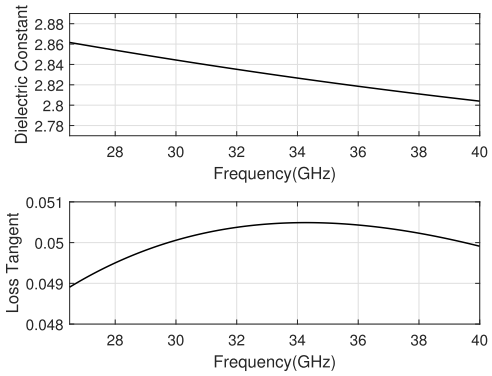

Fig. 3. Formlabs Flexible 80A material characterization results. Top: dielectric constant versus frequency. Bottom: loss tangent versus frequency.

pressure to the deployed structure from the top of the snapping segment, initially, the displacement versus force is linear. When pressure reaches 0.83 N/M^2, the snapping segment will rapidly conform to the bearing segment, and the structure will reach its second stable "retracted" state. In general, the stiffness of the element structure can be controlled by t_1 and t_2; for smaller values of t_1 and t_2, the lower values of external forces will be needed to retract the structure, but if t_1 and t_2 are too small, the printability will be reduced. Fig. 2(b) shows how large the element height h needs to be to cover the full 360° phase shift when sweeping the values of t_1, t_2, and t_3 from -60% to 60% away from the baseline used for the design. When decreasing the value of t_1, t_2, or t_3, the dielectric density of the element will be reduced, thus decreasing the effective dielectric constant; additional height h will be required for the same amount of phase delay. For larger values of angle α, the snapping segment will tend to lock onto the bearing segment more securely; while for vary small values of angle α, the structure can "pop-up" automatically when the external forces are removed.

B. RF Design

The Formlabs Flexible 80A material is characterized using the Nicolson–Ross–Weir (NRW) methodology with 3-D-printed WR28 waveguide samples and A-INFO 28CLKA2 waveguide calibration kit. The characterization results are shown in Fig. 3, and the dielectric constant at 30 GHz is 2.763 with a loss tangent of 0.042.

The element with dimensions discussed in Section II-A is designed and simulated in CST Studio Suite 2019 frequency domain solver with unit cell boundary conditions and Floquet port excitation. The phase delay of one element can be tuned by varying the height h [Fig. 1(a)]. The simulated phase response and reflection coefficient with respect to different angle of incidence (AoI) are shown Figs. 4 and 5. The phase fluctuations in Fig. 4 are caused by the combination of incident and reflected waves. A full 360° phase shift can be obtained by changing the element height h from 8.00 to 29.87 mm when $AoI = 0°$. The simulation data are processed with a linear interpolative curve fitting algorithm to ensure any desired phase value can be matched with a precise element height. It can be observed in Fig. 4 that the phase response

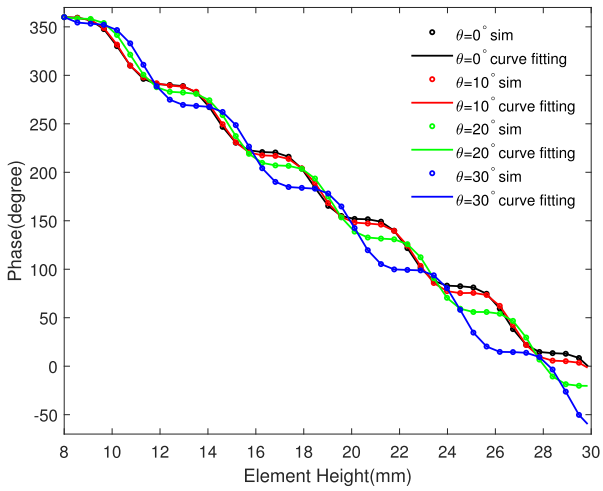

Fig. 4. Simulated phase response versus element height for different AoI values at 30 GHz.

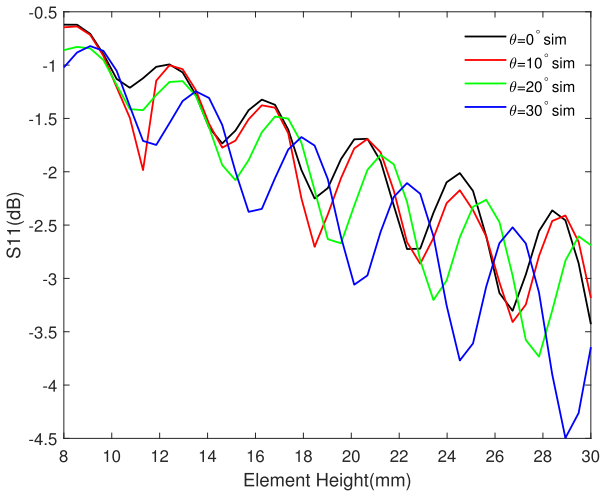

Fig. 5. Simulated reflection coefficient versus element height for different AoI values at 30 GHz.

of the dielectric element will be changed under different oblique incident angles, introducing phase errors to the design. Thus, it is critical to optimize the phase distribution efficiently to realize wide beam-scanning abilities and minimize the array's overall phase error with the optimization process to be discussed in Section III.

III. Reflectarray Design, Fabrication, and Measurement

A. Reflectarray Design

1) Bifocal Phase Distribution: To achieve a reconfigurable radiation pattern for a reflectarray antenna, various beam-scanning methodologies can be utilized. One common approach is by introducing active components, e.g., use RF diodes/switches to turn the element on and off [21], [22], use electric motors to tune the phase response of each element [23], [24], or use tunable loading materials, such as graphite [25], fluids [26], and so on. The active tuning approach can be fast and accurate and achieves a wide range of scanning angles. However, the active components can be bulky and expensive and require a complex feeding circuit. As a

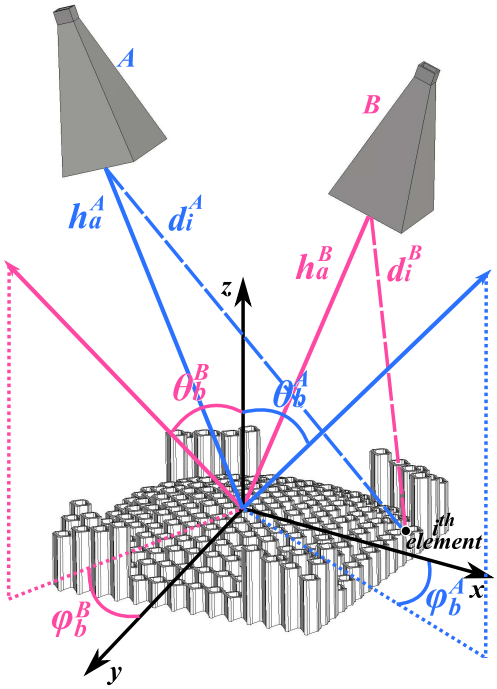

Fig. 6. Schematic of the bifocal beam scanning reflectarray setup.

result, the reflectarray can be unreliable, difficult to fabricate, and occupy a significant larger volume. Another approach to achieve reconfigurable pattern is by rotating the excitation antenna [5], [6], [7]. In contrast, no active component is required so the design can be low cost, easy to fabricate, and maintain a constant volume.

In this article, we use a well-studied bifocal method [7] to realize a wide beam scanning range with uniform gain response across different scanning angles when rotating the feed horn antenna from point A to point B, as shown in Fig. 6. Two yz plane symmetrical feed horn antenna positions define the two focal points for the reflectarray. The ideal phase shifting value of the ith element $\phi(x_i, y_i)$ at any given position (x_i, y_i) with respect to feed horn antenna A or B can be calculated by

$$\phi(x_i, y_i)^{A/B} = k_0\left(d_i^{A/B} - \left(x_i cos\left(\varphi_b^{A/B}\right) + y_i sin\left(\varphi_b^{A/B}\right)\right) sin\left(\theta_b^{A/B}\right)\right) \quad (1)$$

$$d_i^{A/B} = \sqrt{\left(x_i - h_a^{A/B} sin\left(\theta_b^{A/B}\right)\right)^2 + y_i^2 + \left(h_a^{A/B} cos\left(\theta_b^{A/B}\right)\right)^2} \quad (2)$$

where k_0 is the propagation constant in vacuum at the center frequency of the design; d_i is the distance between feed horn A/B phase center and element i; φ_b is the azimuth angle of the main beam with respect to the x-axis, and θ_b is the elevation angle of the main beam with respect to the z-axis. To simplify the problem, we set $\varphi_b^{A/B} = 0°$. In this design, we choose $\theta_b^A = -30°$, $\theta_b^B = 30°$, and $h_a^A = h_a^B = 240$ mm. The ideal phase response can be written as

$$\phi(x_i, y_i)^A = k_0\left(d_i^A - x_i sin\left(\theta_b^A\right)\right) \quad (3)$$

$$\phi(x_i, y_i)^B = k_0\left(d_i^B - x_i sin\left(\theta_b^B\right)\right). \quad (4)$$

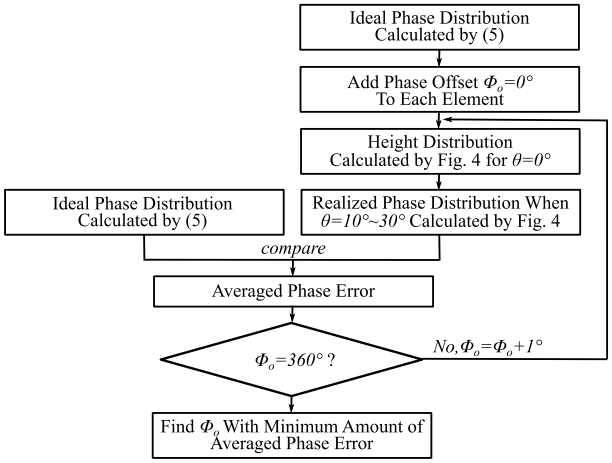

Fig. 7. Schematic of the phase optimization program.

For bifocal reflectarray design, the required phase for the ith element will be an averaged value of the ideal phases

$$\phi(x_i, y_i) = \frac{\phi(x_i, y_i)^A + \phi(x_i, y_i)^B}{2}. \quad (5)$$

2) Phase Optimization: As discussed in Section II, the phase response of every individual dielectric element will change significantly depending on the AoI value. Typically, the reflectarray is designed based on the AoI = 0° simulation results. Thus, significant phase error will be introduced as the feed horn antenna rotates, and the performance of the reflectarray will be compromised. To alleviate this issue, the optimization algorithm shown in Fig. 7 is developed to minimize the overall phase error.

The initial reflectarray design with the appropriate element heights relies on the "ideal" phase distribution calculated by (5); then, a compensating fixed phase offset ϕ_o is added to all elements. With this added phase offset, the height distribution of the array calculated by Fig. 4 for $\theta = 0°$ will be different from the design without a phase offset. Next, we evaluate the realized phase distribution calculated by Fig. 4 under different incident angles and compare this realized phase distribution with the ideal case calculated by (5); thus, we can obtain the averaged phase error for a certain phase offset ϕ_o. By repeating the process for ϕ_o values increasing by 1° over the range of 0°–360°, the ϕ_o value featuring the minimum amount of averaged phase error over all different elements with respect to the ideal phase distribution can be identified, thus defining the corresponding compensated phase distribution and height distribution.

In this work, a 118 mm × 118 mm array with 14 × 16 elements is presented. The dimensions of this array are bounded by the size of the build plate on our 3-D printer, and 3-D printers with larger build plate are commercially available to fabricate larger array designs. The utilized excitation is A-INFO LB-180400-20-C-KF wideband horn antenna. The computer aided design (CAD) model of the excitation was imported to CST Studio Suite 2019 for the full-wave simulation to evaluate the performance of the dielectric reflectarray. The output of the optimizer is shown in Fig. 8, and performance comparison between optimized phase

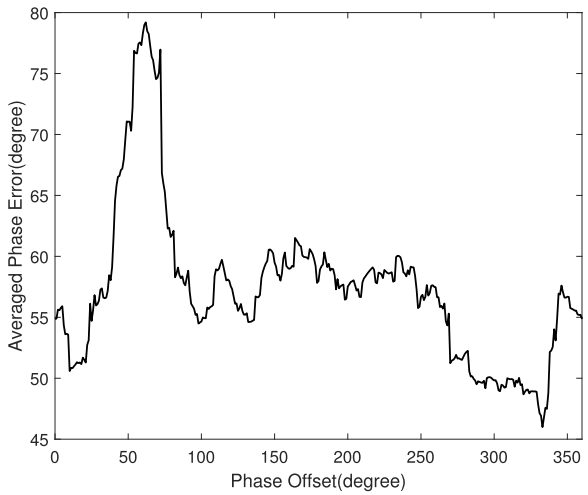

Fig. 8. Output of the phase optimization program: lowest phase error at 333° offset.

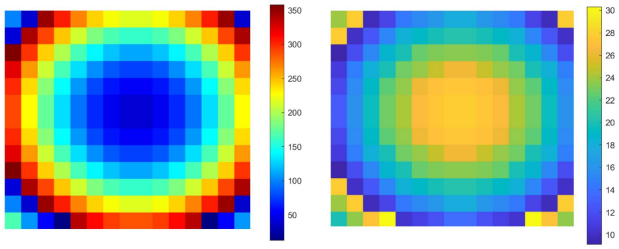

(a) (b)

Fig. 9. (a) Phase distribution of the bifocal reflectarray. (b) Element height distribution of the bifocal reflectarray.

TABLE I
PERFORMANCE COMPARISON OF DIFFERENT PHASE OFFSETS

Phase Offset	333deg (best)	150deg	67deg (worst)
Gain@10deg	24.9dBi	23.3dBi	18.9dBi
SLL@10deg	-20.17dB	-17.34dB	-15.43dB
Gain@30deg	25.0dBi	24.3dBi	20.4dBi
SLL@30deg	-18.5dB	-16.33dB	-13.44dB

offset and other offset values is shown in Table I; the phase distribution calculated by (5) is shown in Fig. 9(a), and the height distribution calculated according to Fig. 4, $\theta = 0°$, is shown in Fig. 9(b).

B. Fabrication

The prototype is fabricated with the Formlabs Form three 3-D printing system. The photosensitive resin Flexible 80A is commercially available with consistent material properties. The prototype is printed flat to avoid internal support structures with ground plane side facing build plate. The 50 μm layer thickness is utilized during the printing, and a wash-and-cure post processing is proceeded after the printing. SLA 3-D-printed samples generally have uncured leftover resin; hence, a 10 min wash in 91% isopropyl alcohol is utilized to remove the extra resin to ensure improved accuracy and surface smoothness. Thereafter, the washed sample will be cured under 60 °C with 405 nm LED lights for 30 min to maximize cross-linking of the photopolymer, optimize structural properties, increase consistency, and reduce electromagnetic losses.

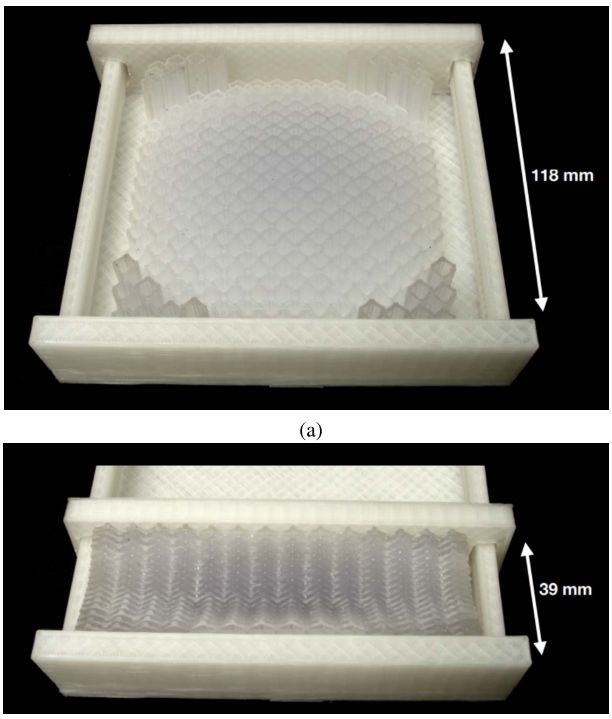

(a)

(b)

Fig. 10. Fabricated sample. (a) Fully deployed sample (front side). (b) Fully retracted sample (back side).

A fabricated prototype is shown in Fig. 10(a), and Fig. 10(b) shows a prototype in a fully retracted state. The fabricated dielectric reflectarray is enclosed by a 3-D-printed frame, and the retracted prototype can be deployed in "one-shot" with a burn switch or a mechanical switch. The retracted prototype shows a 65% volume reduction compared with the fully deployed state.

C. Simulation and Measurement Results

The measurement setup for the beam-scanning dielectric reflectarray is shown in Fig. 11. The reflectarray is held by a 3-D-printed frame with a rotatable arm to tune the scanning angle. Two A-INFO LB-180400-20-C-KF wideband horn antennas are utilized as the excitation and receiver. The distance between the reflectarray and the receiver is 1.70 m.

The simulated and measured realized gain versus scan angles are shown in Fig. 12(a). The simulation and measurement data show good matching, and the optimized bifocal design shows controlled gain variation behavior with less than 1 dB. The broadside beam (zero scan angle) is not studied due to the aperture blockage effects from the feed antenna. The measured realized gain versus frequency is shown in Fig. 12(b).

Fig. 13 shows the simulated and measured radiation patterns across $-10°$ to $-30°$ scan angles with 10° resolution. Fig. 14 shows the simulated and measured radiation patterns across 10°–30° scan angles with 10° resolution. The optimized bifocal reflectarray shows stable gain pattern and a good sidelobe level (SLL) response. The SLL in simulation varies

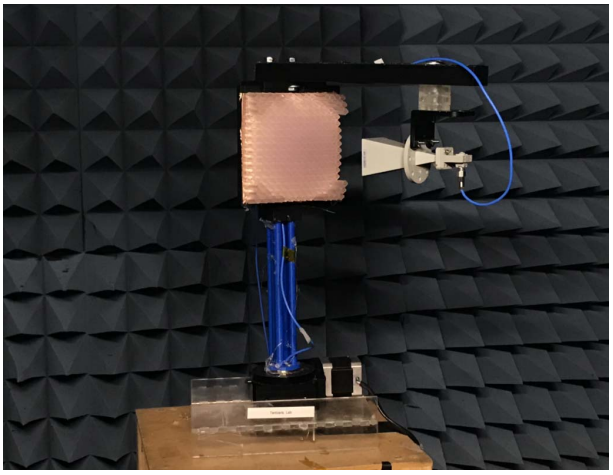

Fig. 11. Measurement setup.

TABLE II
SUMMARY OF THE MEASUREMENT RESULTS AT 30 GHz

Scan Angle (deg)	-30	-20	-10	10	20	30
Realized Gain (dBi)	24.9	25.5	24.7	24.6	25.7	24.7
SLL (dB)	-19.46	-17.32	-18.22	-19.39	-17.77	-18.39
3dB Beamwidth (deg)	6.1	6.4	7.2	7.1	6.2	5.9
1dB Bandwidth (%)	25.4	21.4	18.7	17.5	21.8	25.2

TABLE III
STATE-OF-THE-ART COMPARISON

Design	[16]	[13]	[14]	[7]	This Work
Frequency	35GHz	30GHz	31GHz	32GHz	30GHz
Size	$153.9\lambda^2$	$144.0\lambda^2$	$154.0\lambda^2$	$227.0\lambda^2$	$129.3\lambda^2$
Realized Gain	23.9dBi	28.0dBi	28.3dBi	30.32dBi	24.6dBi
1dB Bandwidth	NA	10.0%	5.2%	4.3%	17.5%
Dielectric	Y	Y	Y	N	Y
Bi-focal	N	N	N	$\pm 30°$	$\pm 30°$
Deployability	N	N	N	N	Y
Aperture Efficiency	12.7%	34.8%	29.0%	37.6%	22.8%

from -20.8 to -17.68 dB, while the measured SLL varies from -19.46 to -17.32 dB. The SLL performance is mainly impacted by the resolution and accuracy of the 3-D printer. The photosensitive resin tends to be overcured when print long tube-shaped structures, causing the sidewall to be thicker than the design. In addition, the long RF cable used during the measurement may impact the VNA's effective dynamic range that causes SLL discrepancy. Despite the slightly increased SLL, the measurement result show a close agreement with the simulation.

The realized gain, SLL, beamwidth, and bandwidth versus scan angles are summarized in Table II. The prototype shows promising and consistent performance across the entire beam scan range.

The measured performance of the dielectric reflectarray design presented in this article is compared with the state-of-the-art reflectarrays at similar frequency ranges shown in Table III, while the proposed design demonstrates widest bandwidth with good radiation performance. The aperture efficiency drop is mainly caused by the dielectric losses from

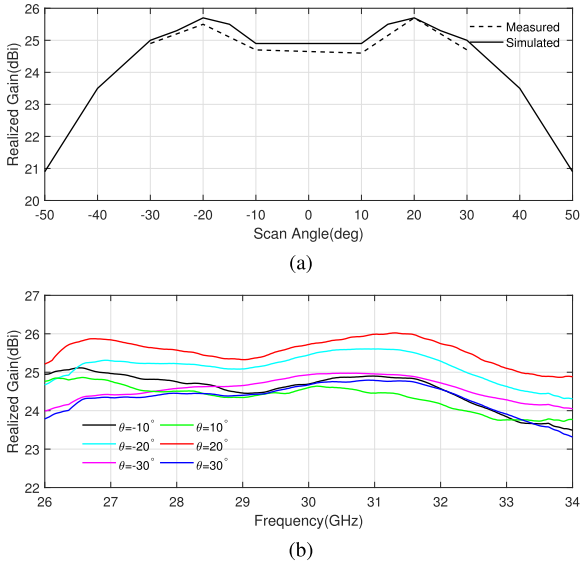

Fig. 12. (a) Simulated and measured realized gain versus scanning angle at 30 GHz. (b) Measured realized gain versus frequency at different scanning angles.

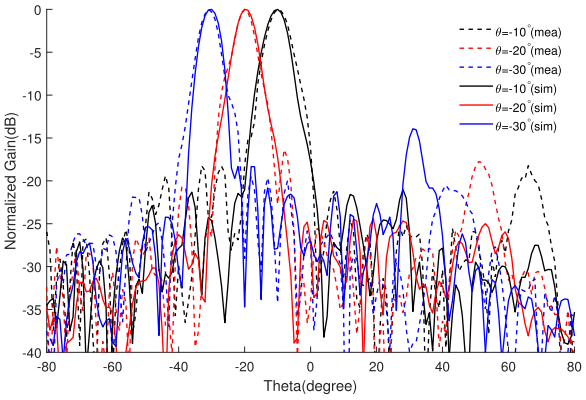

Fig. 13. Measured and simulated radiation patterns at 30 GHz with the scan angles from $-10°$ to $-30°$.

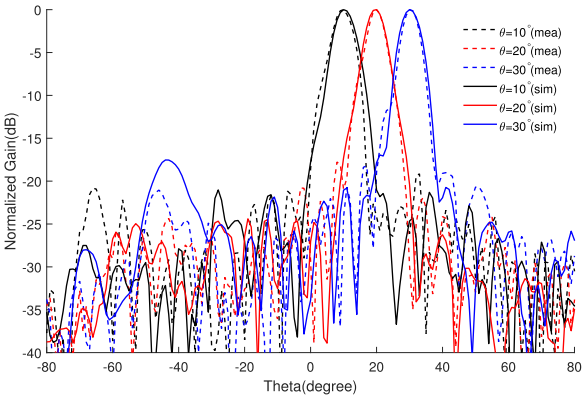

Fig. 14. Measured and simulated radiation patterns at 30 GHz with the scan angles from 10° to 30°.

the material. This issue could potentially be improved by utilizing a low-loss flexible polymer. Another reason of the efficiency drop is the fact that when the excitation horn antenna rotates from 30° to 10°, the edge illumination of the array will drop from −3 to −8.5 dB as the feed horn antenna has an E-plane −3 dB beamwidth of 14°, and the feed center from the horn to the reflectarray is 240 mm. The proposed reflectarray is the only one offering beam-scanning ability, deployability, and full dielectric design simultaneously.

IV. Conclusion

This article demonstrated a state-of-the-art deployable, beam-scanning dielectric reflectarray enabled by kirigami-inspired element structures. The design is realized by the low-cost commercialized SLA 3-D printing system with the flexible photopolymer. The realized prototype demonstrated high realized gain, wide-bandwidth, −10° to −30° and 10° to 30° of scan range, and 65% of volume reduction when retracted, enabling more space-limited high-end communication applications for dielectric reflectarrays. The flexible element structure can potentially introduce multistage reconfigurability to the design of dielectric reflectarray in future work.

Acknowledgment

The authors would like to thank the National Science Foundation (NSF), Alexandria, VA, USA, and Air Force Office of Scientific Research (AFOSR), Arlington, VA, for supporting this work.

References

[1] J. Huang, *Reflectarray Antennas*. Hoboken, NJ, USA: Wiley, Oct. 2007. [Online]. Available: https://www.xarg.org/ref/a/047008491X/

[2] A. J. Rubio, A.-S. Kaddour, N. Brown, L. L. Howell, S. P. Magleby, and S. V. Georgakopoulos, "A physically reconfigurable origami reflectarray based on the augmented square twist pattern," in *Proc. IEEE Texas Symp. Wireless Microw. Circuits Syst. (WMCS)*, May 2021, pp. 1–4.

[3] M. Cooley *et al.*, "RF design and development of a deployable membrane reflectarray antenna for space," in *Proc. IEEE Int. Symp. Phased Array Syst. Technol. (PAST)*, Oct. 2019, pp. 1–4.

[4] R. E. Hodges, N. Chahat, D. J. Hoppe, and J. D. Vacchione, "A deployable high-gain antenna bound for mars: Developing a new folded-panel reflectarray for the first CubeSat mission to Mars," *IEEE Antennas Propag. Mag.*, vol. 59, no. 2, pp. 39–49, Apr. 2017.

[5] G.-B. Wu, S.-W. Qu, and S. Yang, "Wide-angle beam-scanning reflectarray with mechanical steering," *IEEE Trans. Antennas Propag.*, vol. 66, no. 1, pp. 172–181, Jan. 2018.

[6] S. R. Rengarajan, "Scanning and defocusing characteristics of microstrip reflectarrays," *IEEE Antennas Wireless Propag. Lett.*, vol. 9, pp. 163–166, 2010.

[7] P. Nayeri, F. Yang, and A. Z. Elsherbeni, "Bifocal design and aperture phase optimizations of reflectarray antennas for wide-angle beam scanning performance," *IEEE Trans. Antennas Propag.*, vol. 61, no. 9, pp. 4588–4597, Sep. 2013.

[8] Y. Qu, C. Guo, W. Peng, J. Ding, Y. Gao, and Y. Song, "Design of a bifocal single reflectarray antenna with improving beam scanning performance," *Open Electr. Electron. Eng. J.*, vol. 9, no. 1, pp. 200–207, Jul. 2015.

[9] E. Martinez-de-Rioja, J. A. Encinar, and G. Toso, "Bifocal dual-reflectarray antenna to generate a complete multiple spot beam coverage for satellite communications in Ka-band," *Electronics*, vol. 9, no. 6, p. 961, Jun. 2020. [Online]. Available: https://www.mdpi.com/2079-9292/9/6/961

[10] F. Yang *et al.*, "Reflectarray design at infrared frequencies: Effects and models of material loss," *IEEE Trans. Antennas Propag.*, vol. 60, no. 9, pp. 4202–4209, Sep. 2012.

[11] P. Nayeri *et al.*, "3D printed dielectric reflectarrays: Low-cost high-gain antennas at sub-millimeter waves," *IEEE Trans. Antennas Propag.*, vol. 62, no. 4, pp. 2000–2008, Apr. 2014.

[12] R. Deng, F. Yang, S. Xu, and M. Li, "Radiation performances of conformal dielectric reflectarray antennas at sub-millimeter waves," in *Proc. IEEE Int. Conf. Microw. Millim. Wave Technol. (ICMMT)*, vol. 1, Jun. 2016, pp. 217–219.

[13] S. Zhang, "Three-dimensional printed millimetre wave dielectric resonator reflectarray," *IET Microw., Antennas Propag.*, vol. 11, no. 14, pp. 2005–2009, 2017.

[14] M. H. Jamaluddin *et al.*, "Design, fabrication and characterization of a dielectric resonator antenna reflectarray in Ka-band," *Prog. Electromagn. Res. B*, vol. 25, pp. 261–275, 2010.

[15] F. Ahmadi, K. Forooraghi, Z. Atlasbaf, and B. Virdee, "Dual linear-polarized dielectric resonator reflectarray antenna," *IEEE Antennas Wireless Propag. Lett.*, vol. 12, pp. 635–638, 2013.

[16] Y.-X. Sun and K. W. Leung, "Millimeter-wave substrate-based dielectric reflectarray," *IEEE Antennas Wireless Propag. Lett.*, vol. 17, no. 12, pp. 2329–2333, Dec. 2018.

[17] M. Abd-Elhady, W. Hong, and Y. Zhang, "A Ka-band reflectarray implemented with a single-layer perforated dielectric substrate," *IEEE Antennas Wireless Propag. Lett.*, vol. 11, pp. 600–603, 2012.

[18] Y. Cui, S. A. Nauroze, R. Bahr, and E. M. Tentzeris, "3d printed one-shot deployable flexible 'kirigami' dielectric reflectarray antenna for mm-wave applications," in *IEEE MTT-S Int. Microw. Symp. Dig.*, Aug. 2020, pp. 1164–1167.

[19] A. Rafsanjani, A. Akbarzadeh, and D. Pasini, "Snapping mechanical metamaterials under tension," *Adv. Mater.*, vol. 27, pp. 5931–5935, Oct. 2015.

[20] T. Castle, D. M. Sussman, M. Tanis, and R. D. Kamien, "Additive lattice kirigami," *Sci. Adv.*, vol. 2, no. 9, Sep. 2016, Art. no. e1601258. [Online]. Available: https://advances.sciencemag.org/content/2/9/e1601258

[21] J. Han, L. Li, G. Liu, Z. Wu, and Y. Shi, "A wideband 1 bit 12×12 reconfigurable beam-scanning reflectarray: Design, fabrication, and measurement," *IEEE Antennas Wireless Propag. Lett.*, vol. 18, no. 6, pp. 1268–1272, Jun. 2019.

[22] M.-T. Zhang *et al.*, "Design of novel reconfigurable reflectarrays with single-bit phase resolution for Ku-band satellite antenna applications," *IEEE Trans. Antennas Propag.*, vol. 64, no. 5, pp. 1634–1641, May 2016.

[23] X. Yang *et al.*, "A broadband high-efficiency reconfigurable reflectarray antenna using mechanically rotational elements," *IEEE Trans. Antennas Propag.*, vol. 65, no. 8, pp. 3959–3966, Aug. 2017.

[24] X. Yang *et al.*, "A mechanically reconfigurable reflectarray with slotted patches of tunable height," *IEEE Antennas Wireless Propag. Lett.*, vol. 17, no. 4, pp. 555–558, Apr. 2018.

[25] T. Niu, J. Zhang, L. Cheng, P. Cao, R. Cui, and Z. Mei, "Reconfigurable terahertz reflectarray based on graphene radiating patches," in *Proc. 14th Eur. Conf. Antennas Propag. (EuCAP)*, Mar. 2020, pp. 1–4.

[26] S. A. Long and G. H. Huff, "A fluidic loading mechanism for phase reconfigurable reflectarray elements," *IEEE Antennas Wireless Propag. Lett.*, vol. 10, pp. 876–879, 2011.

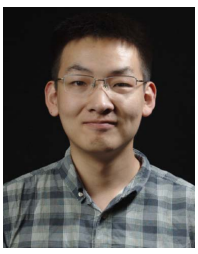

Yepu Cui (Student Member, IEEE) received the B.S. degree in electrical engineering from the Harbin Institute of Technology, Harbin, China, in 2017. He is currently pursuing the Ph.D. degree with the School of Electrical and Computer Engineering, Georgia Institute of Technology, Atlanta, GA, USA.

His research interests include the design of novel origami-inspired reconfigurable antennas and microwave components using additive manufacturing processes, such as inkjet and 3-D printing technologies.

Prof. Cui is a member of the ATHENA Research Group.

Ryan Bahr received the B.S. degree *(summa cum laude)* from the Georgia Institute of Technology, Atlanta, GA, USA, in 2013, with a focus on RF engineering, and the M.S. degree from the Georgia Institute of Technology in 2015 with a focus on electromagnetics and a minor in computer science.

He is currently a Research Assistant with the ATHENA Research Laboratory, Georgia Institute of Technology, where he is involved in focusing on the development of 3-D electromagnetic designs utilizing additive manufacturing. He is also involved in designing complex electromagnetic structures, where additive manufacturing utilizes technologies, such as fused deposition modeling, stereolithography (SLA), and inkjet printing. His research interest include mathematically inspired structures, inkjet printing of flexible electronics, and the utilization of additive manufacturing for RF packaging and mm-wave electronics.

Prof. Bahr received the Best Student Poster Award at Gomac Tech 2016 for Additively Manufactured Flexible and Origami-Reconfigurable RF Sensors.

Syed A. Nauroze received the B.Sc. degree (Hons.) in computer engineering from the University of Engineering and Technology, Taxila, Pakistan, in 2005, and the M.Sc. degree in electrical engineering from the KTH Royal Institute of Technology, Stockholm, Sweden, in 2008. He is currently pursuing the Ph.D. degree in electrical and computer engineering with the Georgia Institute of Technology, Atlanta, GA, USA.

From 2008 to 2009, he was with the Microsystems Technology Laboratory, KTH Royal Institute of Technology, where he conducted research on on-chip millimeter-wave antennas for automotive radar and future wireless applications. He has a teaching experience of seven years. He is currently a Research Assistant with the ATHENA Laboratory, Georgia Institute of Technology. His current research interests include the application of additive manufacturing techniques, such as 3-D printing and ink-jet printing for flexible and origami-based RF structures.

Dr. Nauroze was a recipient of the Prestigious Swedish Institute Scholarship in 2006 and the Fulbright Scholarship in 2014 for his master's and Ph.D. degrees, respectively.

Tingyu Cheng is currently pursuing the Ph.D. degree in human-centered computing with the Georgia Institute of Technology, Atlanta, GA, USA, with a focus on digital fabrication of soft actuators and circuits.

Thamer S. Almoneef (Member, IEEE) received the B.S. degree in electrical and computer engineering from Dalhousie University, Halifax, NS, Canada, in 2009, and the M.A.Sc. and Ph.D. degrees in electrical and computer engineering from the University of Waterloo, Waterloo, ON, Canada, in 2012 and 2017, respectively.

In 2012, he was appointed as a Lecturer with Prince Sattam Bin Abdulaziz University, Al-Kharj, Saudi Arabia, where he is currently an Associate Professor with the Department of Electrical and Computer Engineering. He has authored or coauthored more than 35 refereed journals and conference papers. His research interests include antenna theory, metamaterials and its wide range applications, metamaterial absorbers, electrically small resonators, rectennas, microwave sensors and imagers, electromagnetic energy harvesting, and renewable energy.

Dr. Almoneef received the scholarship from Prince Sattam Bin Abdulaziz University to pursue his Ph.D. studies.

Manos M. Tentzeris (Fellow, IEEE) received the Diploma degree *(magna cum laude)* in electrical and computer engineering from the National Technical University of Athens, Athens, Greece, and the M.S. and Ph.D. degrees in electrical engineering and computer science from the University of Michigan, Ann Arbor, MI, USA, in 1993 and 1998, respectively.

He was a Visiting Professor with the Technical University of Munich, Munich, Germany, in 2002, the Georgia Tech Research Institute (GTRI), Athlone, Ireland, in 2009, and the Laboratory for Analysis and Architecture of System (LAAS-CNRS), Toulouse, France, in 2010. He is currently a Ken Byers Professor in flexible electronics with the School of Electrical and Computer Engineering, Georgia Institute of Technology, Atlanta, GA, USA, where he is also the Head of the ATHENA Research Group (20 researchers) and the GTECE Electromagnetics Technical Interest Group, an Associate Director of the RFID/Sensors Research, Georgia Electronic Design Center, the Associate Director of the RF Research, National Science Foundation (NSF)-Packaging Research Center, and as the RF Alliance Leader. He has helped in developing academic programs in 3-D/inkjet-printed RF electronics and modules, flexible electronics, origami and morphing electromagnetics, highly integrated/multilayer packaging for RF and wireless applications using ceramic and organic flexible materials, paper-based RFID's and sensors, wireless sensors and biosensors, wearable electronics, "Green" electronics, energy harvesting and wireless power transfer, nanotechnology applications in RF, microwave MEMS, and system on package (SOP)-integrated (UWB, multiband, mmW, and conformal) antennas. He has authored more than 650 papers in refereed journals and conference proceedings, five books, and 25 book chapters.

Dr. Tentzeris is a member of the URSI-Commission D and the MTT-15 Committee, an Associate Member of European Microwave Association (EuMA), a fellow of the Electromagnetic Academy, and a member of the Technical Chamber of Greece. He was a recipient/co-recipient of the 2019 Humboldt Research Award, the 2018 Intel IEEE Electronic Components and Technology Conference (ECTC) 2018 Best Student Paper Award, the 2017 Georgia Institute of Technology Outstanding Achievement in Research Program Development Award, the 2016 Bell Labs Award Competition 3rd Prize, the 2015 IET Microwaves, Antennas, and Propagation Premium Award, the 2014 Georgia Institute of Technology Electrical and Computer Engineering (ECE) Distinguished Faculty Achievement Award, the 2014 IEEE RFID Technology and Application (RFID-TA) Best Student Paper Award, the 2013 IET Microwaves, Antennas and Propagation Premium Award, the 2012 FiDiPro Award in Finland, the inter-company marketing group (iCMG) Architecture Award of Excellence, the 2010 IEEE Antennas and Propagation Society Piergiorgio L. E. Uslenghi Letters Prize Paper Award, the 2011 International Workshop on Structural Health Monitoring Best Student Paper Award, the 2010 Georgia Institute of Technology Senior Faculty Outstanding Undergraduate Research Mentor Award, the 2009 IEEE TRANSACTIONS ON COMPONENTS AND PACKAGING TECHNOLOGIES Best Paper Award, the 2009 E. T. S. Walton Award from the Irish Science Foundation, the 2007 IEEE AP-S Symposium Best Student Paper Award, the 2007 IEEE Microwave Theory and Techniques Society (MTT-S) International Microwave Symposium (IMS) Third Best Student Paper Award, the 2007 International Symposium on Antennas and Propagation (ISAP) 2007 Poster Presentation Award, the 2006 IEEE MTT-S Outstanding Young Engineer Award, the 2006 Asia–Pacific Microwave Conference Award, the 2004 IEEE TRANSACTIONS ON ADVANCED PACKAGING Commendable Paper Award, the 2003 National Aeronautics and Space Administration (NASA) Godfrey "Art" Anzic Collaborative Distinguished Publication Award, the 2003 International Bank of Commerce (IBC) International Educator of the Year Award, the 2003 IEEE Components, Packaging, and Manufacturing Technology (CPMT) Outstanding Young Engineer Award, the 2002 International Conference on Microwave and Millimeter-Wave Technology Best Paper Award (Beijing, China), the 2002 Georgia Institute of Technology–ECE Outstanding Junior Faculty Award, the 2001 Applied Computational Electromagnetics Society (ACES) Conference Best Paper Award, the 2000 NSF CAREER Award, and the 1997 Best Paper Award of the International Hybrid Microelectronics and Packaging Society. He was the Co-Chair of the 2019 IEEE APS Conference, the TPC Chair of the IEEE MTT-S IMS 2008 Symposium, and the Chair of the 2005 IEEE Computational Electromagnetics in Time-Domain (CEM-TD) Workshop. He is the Vice-Chair of the RF Technical Committee (TC16) of the IEEE CPMT Society. He is the Founder and the Chair of the RFID Technical Committee (TC24) of the IEEE MTT-S and the Secretary/Treasurer of the IEEE C-RFID. He has given more than 100 invited talks to various universities and companies all over the world. He served as one of the IEEE MTT-S Distinguished Microwave Lecturers from 2010 to 2012 and is one of the IEEE C-RFID Distinguished Lecturers. He is an Associate Editor of the IEEE TRANSACTIONS ON MICROWAVE THEORY AND TECHNIQUES, the IEEE TRANSACTIONS ON ADVANCED PACKAGING, and the *International Journal on Antennas and Propagation*.